Mio-Pliocene aridity in the south-central Andes associated with Southern Hemisphere cold periods

William H. Amidon[a,1], G. Burch Fisher[b,c], Douglas W. Burbank[c], Patricia L. Ciccioli[d], Ricardo N. Alonso[e], Andrew L. Gorin[a], Perri H. Silverhart[a], Andrew R. C. Kylander-Clark[c], and Michael S. Christoffersen[b]

[a]Geology Department, Middlebury College, Middlebury, VT 05753; [b]Jackson School of Geosciences, University of Texas at Austin, Austin, TX 78712; [c]Earth Research Institute, University of California, Santa Barbara, CA 93106; [d]Departamento de Ciencias Geológicas, Instituto de Geociencias Básicas, Aplicadas y Ambientales de Buenos Aires, Facultad de Ciencias Exactas y Naturales, Universidad de Buenos Aires-Consejo Nacional de Investigaciones Científicas y Técnicas, Buenos Aires C1428EHA, Argentina; and [e]Instituto Superior de Correlación Geológica, Universidad Nacional de Salta-Consejo Nacional de Investigaciones Científicas y Técnicas, 4400 Salta, Argentina

Edited by Thure E. Cerling, University of Utah, Salt Lake City, UT, and approved May 12, 2017 (received for review January 9, 2017)

Although Earth's climate history is best known through marine records, the corresponding continental climatic conditions drive the evolution of terrestrial life. Continental conditions during the latest Miocene are of particular interest because global faunal turnover is roughly synchronous with a period of global glaciation from ∼6.2–5.5 Ma and with the Messinian Salinity Crisis from ∼6.0–5.3 Ma. Despite the climatic and ecological significance of this period, the continental climatic conditions associated with it remain unclear. We address this question using erosion rates of ancient watersheds to constrain Mio-Pliocene climatic conditions in the south-central Andes near 30° S. Our results show two slowdowns in erosion rate, one from ∼6.1–5.2 Ma and another from 3.6 to 3.3 Ma, which we attribute to periods of continental aridity. This view is supported by synchrony with other regional proxies for aridity and with the timing of glacial "cold" periods as recorded by marine proxies, such as the M2 isotope excursion. We thus conclude that aridity in the south-central Andes is associated with cold periods at high southern latitudes, perhaps due to a northward migration of the Southern Hemisphere westerlies, which disrupted the South American Low Level Jet that delivers moisture to southeastern South America. Colder glacial periods, and possibly associated reductions in atmospheric CO_2, thus seem to be an important driver of Mio-Pliocene ecological transitions in the central Andes. Finally, this study demonstrates that paleo-erosion rates can be a powerful proxy for ancient continental climates that lie beyond the reach of most lacustrine and glacial archives.

Messinian | Miocene | Pliocene | M2 | precipitation

Earth's climate has played a fundamental role in the evolution of terrestrial life (1, 2). Whereas marine-based climate records offer broad insights into ancient climates with high temporal resolution (3), it is the associated changes in continental climate that govern the evolution of terrestrial life. Past changes in continental climate, however, are typically difficult to measure and the effect of global climate events on terrestrial life is commonly unclear. For example, how do changes in global temperature translate to changes in the hydrologic cycle at specific locations on Earth? To what extent does averaging of signals in the marine climatic record mask the severity of continental climatic shifts and their impact on terrestrial fauna? Answers to these questions remain particularly elusive for pre-Quaternary climatic events, which are commonly beyond the reach of continental lacustrine or glacial climate proxies. Additional continental climate proxies for the Mio-Pliocene time can thus help reveal the role of global climate excursions in driving well-known faunal transitions.

Continental conditions during latest Miocene cooling are of particular interest, because major faunal turnovers during this time influenced the evolution of many species (4, 5). For example, the late Miocene (∼7.0–5.5 Ma) saw expansion of plant species that use a C4 photosynthetic pathway, which began to outcompete existing C3 plants across subtropical regions of South America, Africa, and Asia (6–8). However, the exact timing and continental climatic conditions that drove this expansion have been the subject of much discussion. C4 plants tend to thrive in warmer conditions, as long as ample moisture is present during the growing season (9). However, because they concentrate CO_2 during photosynthesis, they likely outcompete C3 plants under low-CO_2 and low-temperature conditions, such as during cold glacial periods. For example, at an atmospheric CO_2 concentration of 250 ppm C4 plants would be favored at all growing season temperatures above ∼18 °C (8). It is thus logical to speculate that the late Miocene spread of C4 plants may have resulted from low-CO_2 conditions. Although several studies have argued against reduced global CO_2 in the late Miocene (10, 11), recent work shows a significant decrease beginning around 7 Ma (12, 13).

Although the timing of onset of C4 expansion varies by location, the major shift in $\delta^{13}C$ is commonly observed in the very latest Miocene between ∼6–5.5 Ma (7, 14, 15). This timing is remarkably similar to the timing of the Messinian Salinity Crisis (MSC), in which the Mediterranean Sea shrank and ultimately dried up from 5.96 to 5.33 Ma (16). The cause of the MSC has also been the subject of much debate (17, 18), but recent work argues it was triggered by glacio-eustatic sea-level fall in response to expansion of Antarctic ice sheets at ∼6 Ma (19) and that the period of maximum aridity (the "Messinian gap") corresponds to one or two glacial periods near 5.53 ± 0.06 Ma (16, 20). These glacial periods are part of a long-recognized, but somewhat enigmatic, sequence of latest Miocene glacials between ∼6.2 and 5.5 Ma, which included up to 18 glacial-interglacial cycles on a

Significance

This paper identifies two periods of enhanced aridity that are synchronous with faunal turnovers in southern South America. Close temporal coincidence with marine climate proxies suggests a period of latest Miocene aridity was associated with a global glacial period and the expansion of C4 vegetation. We thus argue that continental aridity in the south-central Andes is associated with cold periods at high southern latitudes and propose a model to link global and regional (continental) climate via shifting of the Southern Hemisphere westerlies. This paper also provides an example of how ^{10}Be paleo-erosion rates can be used as a climate proxy and demonstrates how ^{10}Be and ^{36}Cl can be combined to reduce uncertainties associated with this method.

Author contributions: W.H.A., G.B.F., and D.W.B. designed research; W.H.A., G.B.F., D.W.B., P.L.C., R.N.A., A.L.G., P.H.S., A.R.C.K.-C., and M.S.C. performed research; W.H.A. and G.B.F. analyzed data; and W.H.A. wrote the paper.

The authors declare no conflict of interest.

This article is a PNAS Direct Submission.

[1]To whom correspondence should be addressed. Email: wamidon@middlebury.edu.

This article contains supporting information online at www.pnas.org/lookup/suppl/doi:10.1073/pnas.1700327114/-/DCSupplemental.

41,000-y obliquity-paced timescale (21, 22). Evidence of latest Miocene ice accumulation in both the Northern (23) and Southern Hemispheres (24) suggest these glacial periods were global in nature and could have been associated with CO_2 levels low enough to favor C4 vegetation on a global scale.

Testing whether late Miocene faunal shifts were driven by CO_2 forcing or temperature/ precipitation forcing is difficult given the relative paucity of proxies for continental paleoclimate. Much of our knowledge of latest Miocene terrestrial climate is derived from plant fossils, hydrocarbon biomarkers, and the isotopic composition of paleosoils and fossil teeth, features that are rare or poorly preserved in most sedimentary sections (25, 26). Likewise, most terrestrial sediments are deposited in association with active mountain belts, creating the additional challenge of deconvolving regional climatic signals from local tectonic–orographic signals. These issues are especially challenging in the south-central Andes where a regionally extensive climate transition in the latest Miocene (14, 27, 28) appears synchronous with significant tectonic uplift at this time (29–32). It thus remains unclear whether the timing and extent of latest Miocene landscape ecologic changes in the south-central Andes were primarily controlled by tectonic–orographic effects or by global-scale changes in climate (e.g., refs. 33–35).

This study addresses these questions by using erosion rates of ancient watersheds as a proxy for Mio-Pliocene (~7–2.8 Ma) precipitation in the south-central Andes (~30° S, 68° W). Because erosion rate in semiarid watersheds of the central Andes is primarily correlated with precipitation (36), transient excursions in erosion rate over <400,000-y timescales should be a robust proxy for paleoprecipitation. Erosion rates are estimated by measuring cosmogenic ^{10}Be in ancient fluvial sediments deposited in foreland basin sequences, which record the erosion rate in their source watersheds (37–39). This approach yields a powerful proxy because it integrates landscape processes over a large region (10^4–10^5 km^2) and provides a continuous record that can be precisely dated using magnetostratigraphy and tephrachronology. Our results show two decreases in erosion rate that are synchronous with the latest Miocene glacial period described above and with a second glacial period from roughly 3.6–3.3 Ma. We attribute these slowdowns to enhanced continental aridity during cold periods at high southern latitudes. Finally, we suggest that both latest Miocene aridity and the coeval expansion of C4 vegetation may have been driven by a latest Miocene glacial period and an associated drop in global CO_2.

Study Area and Methods

This section presents a summary of the study area and methods, with full details provided in *SI Appendix*. We developed paleo-erosion-rate records on the Huaco and Toro Negro sections, which were deposited in the central and northern regions of the Bermejo Foreland Basin, respectively (Fig. 1). The two sections were chosen because they are well exposed in deep road cuts, a prerequisite for applying the paleocosmogenic technique. The sections are composed of coarse fluvial sandstones and conglomerates shed from the eastern slopes of the Andes over the last 15 My. A paleomagnetic chronology was developed along the Huaco section, constraining the age of our samples to ~6.4 to ~2.6 Ma (*SI Appendix*, Fig. S2). The Toro Negro section lacks suitable deposits for paleomagnetic dating and has been previously dated to ~7–2.3 Ma by U-Pb zircon dating of tephra (40).

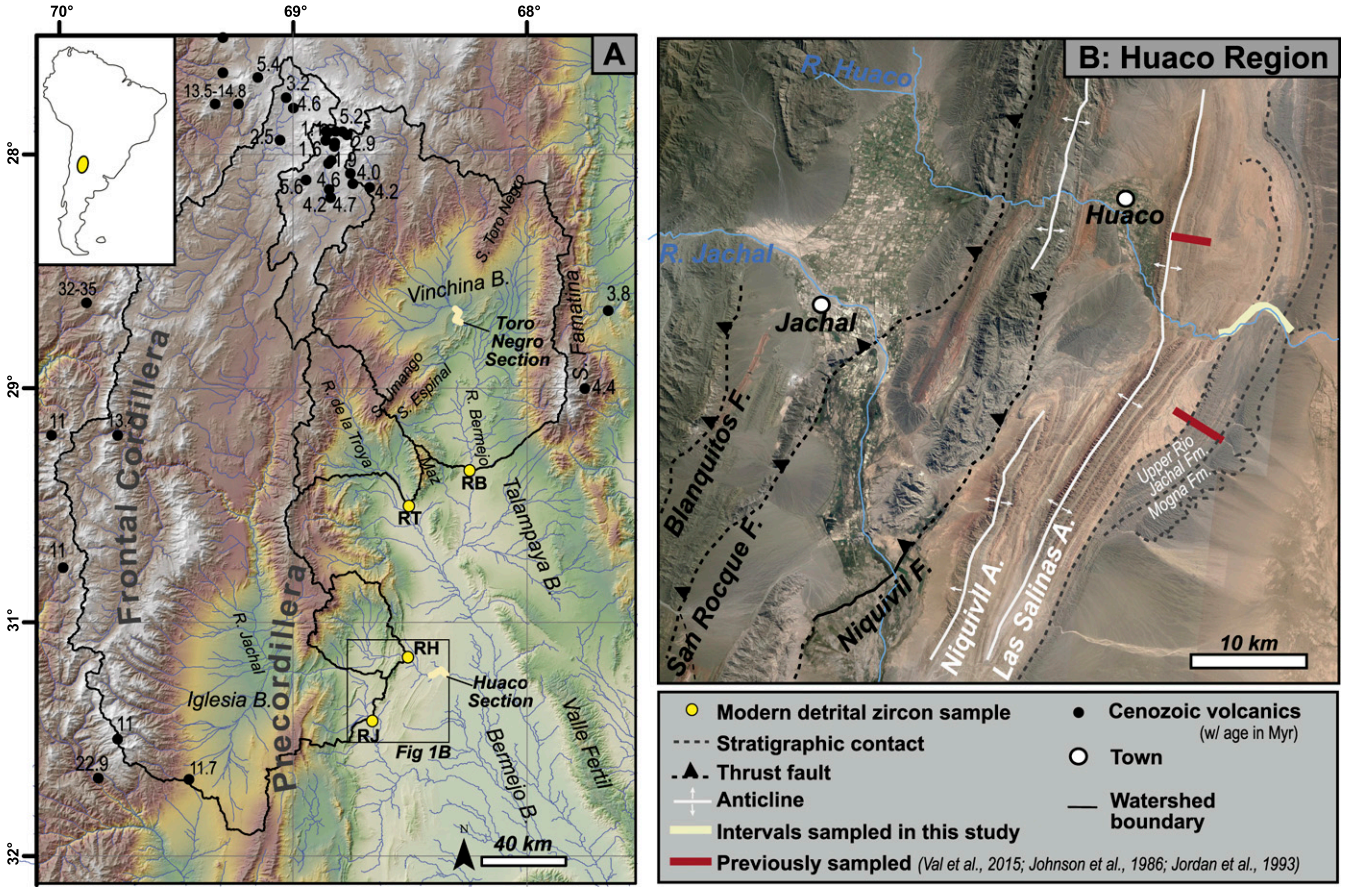

Fig. 1. (*A*) Shaded relief map of the study area derived from a 90-m digital elevation model showing the extent of modern watersheds and a compilation of young volcanic ages (73, 74). (*B*) Satellite image of the Huaco study area showing the location of the sampling transect used in this and previous studies, as well as key tectonic structures (75).

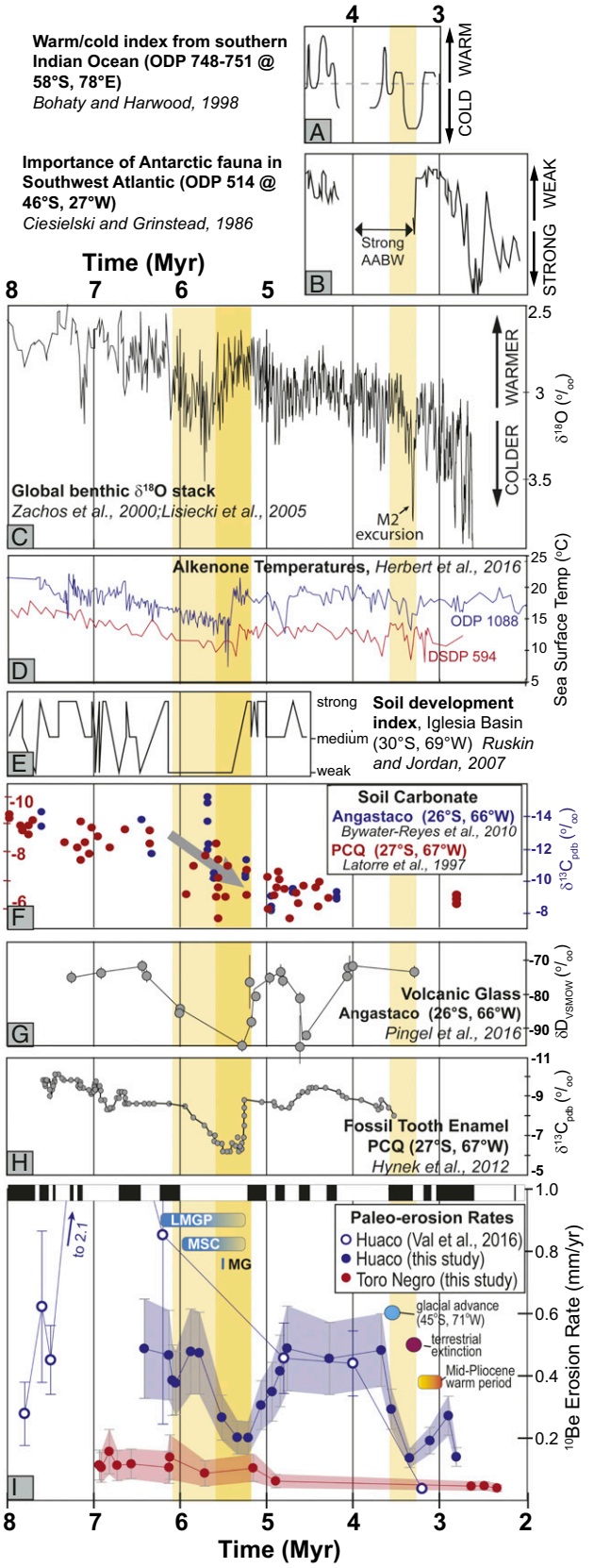

Fig. 2. (*A–H*) Compilation of regional and global climate proxies. (*I*) Paleo-erosion rate records compared with major global and regional climatic events. LMGP denotes the latest Miocene glacial period (20). MSC denotes the Messinian Salinity Crisis (16) MG denotes the Messinian Gap when aridity peaked in the Mediterranean (16). The timing of glaciation, extinction, and the mid-Pliocene warm period are depicted (49, 54, 76). The paleo-erosion rates of Val et al. (38) were also developed on the Huaco section, but along a different sampling transect (see Fig. 1). Larger uncertainties on their dataset result from using surface samples that were not shielded from modern cosmic-ray exposure. Such contrasting sampling strategies may explain disagreement between the two datasets for older samples in which small amounts of modern exposure ($C_{exhumation}$) could swamp the ancient (and significantly decayed) ^{10}Be signal (C_{paleo}).

Samples for measurement of cosmogenic ^{10}Be were collected from sandstones and conglomerates exposed at the base of 3.5- to 6-m-high road cuts to minimize modern cosmogenic nuclide production that could skew paleo-erosion rate estimates. Our approach to estimating paleo-erosion rates in foreland sediments is similar to that originally described by Charreau et al. (37) and also applied in more recent studies (38, 39). Measured ^{10}Be represents the sum of at least three components:

$$C_{paleo} = C_{measured} - C_{burial} - C_{exhumation}. \quad [1]$$

C_{paleo} is the concentration of ^{10}Be accumulated during exposure in the paleo watershed and is the quantity used to estimate paleo-erosion rates. C_{burial} is the amount of ^{10}Be acquired during deposition of the sample and is estimated using the sedimentation rate. $C_{exhumation}$ is the amount of ^{10}Be in the sample acquired during recent exhumation. At Huaco it is estimated using long-term exhumation rates derived from apatite U-Th/He dating (29). At Toro Negro it is estimated from exhumation rates computed from the concentration of muogenic ^{36}Cl in K-rich feldspars. The rationale for this approach is that because sandstone samples have depositional ages >5.15 Ma and ^{36}Cl has a half-life of ∼0.3 Ma, all cosmogenic ^{36}Cl originally created during paleoexposure or burial has decayed away. Likewise, because the samples were collected from shielded depths, modern spallation production is negligible and any measured ^{36}Cl is derived from either radiogenic or muogenic production.

A major assumption of our paleo-erosion approach is that the extent of the watershed and the distribution of quartz-bearing lithologies have not changed significantly over time. This assumption is tested by using U-Pb dating of detrital zircons to establish sediment provenance. Detrital zircon provenance of the Toro Negro section was previously summarized in Amidon et al. (40), who inferred no major changes in provenance. At Huaco, 10 detrital zircon samples were analyzed from the Huaco section and compared with four samples from modern rivers (*SI Appendix*, Figs. S3 and S4). Results show that sedimentary provenance did not change significantly during the period of interest and that sediments in the Huaco section were sourced primarily from Precordillera units immediately to the east (Fig. 1).

Results and Discussion

Evidence for Latest Miocene Aridity. The Huaco record shows generally stable erosion rates of ∼0.5 mm/y marked by two ∼70% slowdowns from ∼6.1–5.2 Ma and ∼3.6–3.3 Ma (Fig. 2*I*). These decreases occur rapidly over timescales of 200,000–400,000 y and are followed by returns to the apparent "background" erosion rate. The slowdowns seem to be robust (e.g., not artifacts of the data), given that successive samples show monotonic increases and decreases, and the data show generally good agreement with the coarser resolution results of Val et al. (38). Likewise, because the slowdowns show rapid recovery of erosion rates on 100,000-y timescales, it seems unlikely they can be explained by changes in the rate or pattern of tectonism, as previously suggested (38). More detailed discussion of tectonic scenarios is presented in *SI Appendix*, section S4. Given that erosion rates in semiarid catchments of the central Andes have been shown to depend primarily on precipitation (36), we equate transient slowdowns in erosion rate to periods of enhanced aridity.

Observations from neighboring regions support the interpretation of enhanced aridity. For example, a period of weak soil development and few preserved paleosols in the Iglesia basin (∼31.5° S) records enhanced aridity between 6.2–5.3 Ma (Fig. 2*E*) (41). Likewise, δD isotopic measurements in volcanic glass suggest a period of aridity in the Angastaco basin (∼25.5° S) from ∼6.3–5.1 Ma (Fig. 2*G*) (28, 35). Inferred aridity is broadly synchronous with carbon isotope excursions thought to record the

expansion of C4 vegetation. For example, $\delta^{13}C$ in paleosol carbonate from the Puerta Corral Quemado section (~28° S) and the Angastaco basin become significantly heavier beginning at ~6 Ma (Fig. 2*F*) (14, 27, 28). In the Puerta Corral Quemado section, $\delta^{13}C$ in fossil tooth enamel shows a well-defined, 3‰ excursion from ~6–5.3 Ma, which is synchronous with our observed slowdown in erosion rates, and with the δD excursion. The fossil tooth record is less noisy than the paleosol record and provides strong evidence of a transient shift toward C4 plants from ~6–5.3 Ma (Fig. 2*H*).

The timing of latest Miocene aridity and $\delta^{13}C$ shifts is broadly synchronous with a global glacial period between 6.2 and 5.5 Ma, inferred from a rapid sea-level drawdown (22, 42, 43), $\delta^{18}O$ in the marine sedimentary record (20, 21), and glacial advances in Greenland (23) and South America (24). Recently, evidence from marine records in the Southern Ocean has provided evidence for major advances of the Antarctic ice sheet beginning about 6 Ma (19). This latest Miocene glacial period created particularly cold conditions at high southern latitudes. Alkenone temperature records from marine cores at 40–50° S show ~5 °C drops in sea-surface temperature between about 7 and 5 Ma, with minima at ~5.5 Ma (Fig. 2*D*). Likewise, a Mio-Pliocene core from Deep Sea Drilling Project (DSDP) site 284 (41° S, 167° E) shows major cooling of bottom waters between ~6.2 and 5.2 Ma, as recorded by the relative proportions of *Neogloboquadrina pachyderma* and *Globigerina falconensis*, which prefer colder and warmer conditions, respectively (44, 45). Finally, the northward limit of ice-rafted debris in Ross Sea sediments shows a major advance in the latest Miocene, interpreted as a northward advance of cold conditions associated with a strengthening Antarctic Polar Front (APF) (46).

The timing of the latest Miocene erosion-rate slowdown at Huaco agrees well with nearby continental proxies (Fig. 2 *E–H*), but the continental proxies are not perfectly synchronous with the global benthic $\delta^{18}O$ stack (Fig. 2*C*). Most notably, the recovery of erosion rate, δD, and $\delta^{13}C$ beginning ~5.3 Ma seems to lag recovery of the $\delta^{18}O$ record by ~0.4 Ma. Taken at face value this offset suggests that aridity and/or low CO_2 in the south-central Andes continued for about 0.4 My after global ice volumes had diminished. However, the minima of Southern Hemisphere sea-surface temperature also lags recovery of the global benthic record by ~0.3 Ma, suggesting that the Southern Hemisphere may have stayed cold for longer or reached peak cold ~0.3 Ma after the peak in Northern Hemisphere ice volume.

Evidence for Mid-Pliocene Aridity. The second slowdown in erosion rates from 3.6–3.3 Ma also corresponds to a period of faunal turnover and glaciation. The slowdown corresponds tightly with the M2 isotope excursion, a 0.75‰ dip in the global benthic $\delta^{18}O$ stack from ~3.5–3.2 Ma (Fig. 2*C*), which presumably records a glacial period (47). Evidence for Southern Hemisphere glaciation comes from glacial till in the southern Andes (46° S) dated to ~3.6 Ma (48). Evidence for aridity comes from a major extinction event observed in the Chapadmalal Cliffs of southeastern Argentina (~38° S, 58° W), in which 53% of species go extinct at ~3.3 Ma (49). This extinction has been attributed to the onset of aridity associated with abrupt changes in the global ocean–atmosphere system (49) and alternatively to an impact event at 3.3 Ma (50). Given sedimentary evidence for aridity in the Chapadmalal Cliffs and the observation of roughly synchronous extinctions in the Uquia Formation of northwestern Argentina (51), we favor a climatic explanation.

Again, aridity and glaciation correspond to cold temperatures at high southern latitudes. A cooling event at ~3.5 Ma is recorded by relative variations of diatoms, silicoflagellates, and radiolarian species in the Southern Ocean, which have varying tolerances for warm vs. cold water (45, 52, 53). For example, changes in faunal abundance reveal a major northward advance of the APF between ~3.7 and 3.2 Ma, suggesting colder conditions over Antarctica during this time. Because the APF exists where the cold waters of the Antarctic displace warmer waters northward, its location is a proxy for Antarctic surface temperature: When Antarctica is colder the APF shifts northward then recedes southward as Antarctica warms (Fig. 3*C*). Ocean Drilling Program (ODP) holes 748–751 in the southernmost Indian Ocean (~58° S, 78° E) record a major northward shift of the APF from 3.6 to 3.2 with a maximum of cold conditions from 3.35 to 3.2 Ma (Fig. 2*A*) (54). Nearby DSDP site 266 (~56° S, 110° E) shows peak "Antarctic" cool conditions between 3.7–3.2 Ma (55). In the southwest Atlantic, ODP hole 514 (~46° S, 27° W) records stratigraphic evidence for intensification of Antarctic bottom water flow (e.g., cooling) from ~3.8–3.2 Ma (Fig. 2*B*) (56).

The correlation between high-latitude temperature and erosion rate continues into the mid-Pliocene warm period, when erosion rates rebounded between ~3.3–2.9 Ma as global temperatures warmed (Fig. 2*I*). The APF migrated ~6° southward during this warm period, and sea-surface temperatures were roughly 3–4° warmer than present (57). In the southwest Atlantic, DSDP hole 514 shows a pronounced shift toward warmer species from roughly 3.15–2.95 Ma (56). In the southern Indian Ocean, ODP holes 748–751 also show a swing back to warmer temperatures from roughly 3.15–3.0 Ma (54). It thus seems that as high southern latitudes temporarily warmed during the mid-Pliocene warm period erosion rates at Huaco rebounded, adding further support for a close link between high-latitude colder temperature and aridity in east-central Argentina.

Global-to-Regional Climate Linkages. When combined with continental and marine proxies, our data suggest that when high southern latitudes were colder conditions in the south-central

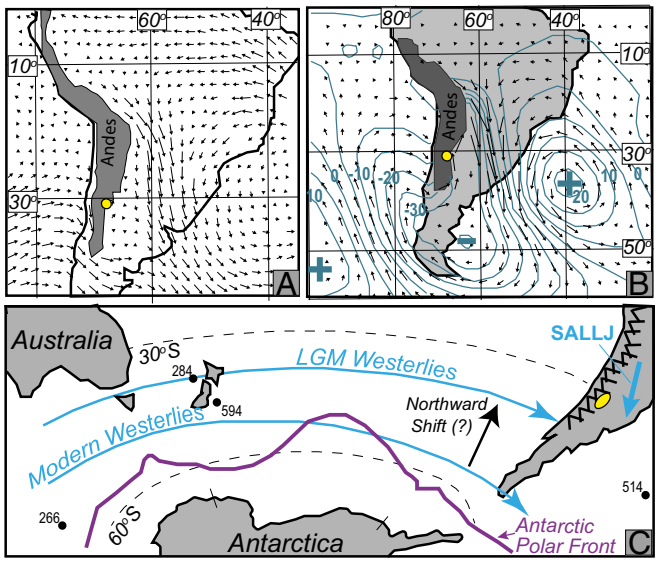

Fig. 3. (*A*) Patterns of low-level winter wind (850 hPa) from 2001 to 2005 based on National Centers for Environmental Prediction reanalysis data, as published in ref. 60. Reproduced from ref. 60. Note the westerlies impinging on the Andes south of 30° S and the easterly trade winds deflected south along the flank of the Andes. Yellow dots denote the Huaco study area in all plots. (*B*) Difference between the mean circulation at 850 hPa and the circulation during a mean Chaco Jet event from 2001 to 2005 as published in ref. 60. Reproduced from ref. 60. Contours of geopotential height anomalies (blue) show the baroclinic wave commonly associated with the Chaco Jet. Note that winds arriving at the study area are primarily southerly and are associated with clockwise circulation around the low pressure system. (*C*) Cartoon showing the hypothetical northward shift of the main westerly flow between modern times and the Last Glacial Maximum.

Andes (25–31° S) were drier. We propose that this aridity represents a breakdown of the atmospheric circulation patterns that bring moisture to the region today. The modern Huaco region receives ~90% of its moisture in the Austral summer (November–March), primarily from wind patterns associated with the South American Low Level Jet (SALLJ) and associated convective recycling (58, 59). The SALLJ is a southward flow of high-velocity winds originating in the Amazon basin (Fig. 3), following trajectories ranging from due south along the flank of the Andes to southeasterly toward Buenos Aires and eastern Argentina (60). Moisture delivered by the SALLJ is subsequently recycled during intense convective storms as warm air rises upward through colder westerly air masses flowing down off high Andean topography (59, 61). Here we use the term "Chaco Jet" interchangeably with SALLJ, considering it to be a particularly strong episode of the SALLJ with deeper southward penetration (62).

The SALLJ is primarily caused by a trough of low pressure that forms on the eastern side of the Andes in response to the setup of baroclinic wave trains over high topography (63–65). Baroclinic waves are changes in upper atmosphere air pressure (<500 hPa) that emanate from the south Pacific and are magnified as the westerlies interact with the orographic barrier of the Andes (64, 66, 67). The intensity and orientation of the SALLJ are thus sensitive to the strength and latitude of the westerly flow and the height and width of Andean topography where the westerlies cross the Andes (Fig. 3*C*). For example, Wang and Fu (66) showed that the intensity of the SALLJ is predicted by the intensity of westerly flow across the Andes at 700 hPa. Likewise, models suggest that as westerlies shift southward over the lower topography of the southernmost Andes the trajectory of the SALLJ becomes more southerly (64).

Given that SALLJ circulation is responsible for most modern precipitation near Huaco and that the SALLJ is itself dependent on the location and strength of the westerlies, we speculate that the ultimate cause of aridity at Huaco was a change in the westerly circulation and/or associated baroclinic waves during periods of high-latitude cold. Geologic evidence shows that the westerlies shifted equatorward during the Last Glacial Maximum (Fig. 3*C*) and would likely have done the same during periods of late Miocene and Pliocene cold (68, 69). If so, the baroclinic pressure trough should shift northward, changing the geometry and/or intensity of the SALLJ and potentially increasing aridity over the eastern Andes from 25 to 31° S.

Colder temperatures may also have directly diminished some of the processes that give rise to the SALLJ and convective recycling of precipitation. For example, colder temperatures in the troposphere during glacial periods are interpreted to have reduced baroclinicity, which would have made it harder to achieve ideal conditions to set up the SALLJ (70, 71). Likewise, colder temperatures in the austral summer may have reduced the vigor of mesoscale convective processes near the downstream end of the SALLJ, which currently strengthens low-level flow of the SALLJ and enhances moisture delivery (72).

Conclusions

Based on ^{10}Be concentrations in foreland basin sediment, we generate a record of paleo-erosion rates in the south-central Andes of Argentina near 30° S. The Huaco record shows two slowdowns in erosion rates: the latest Miocene (6.1–5.3 Ma) and the middle Pliocene (3.6–3.3 Ma). Both slowdowns are followed by rapid returns to a "background" erosion rate, suggesting they are not driven by tectonic reorganization. Given that erosion rates in semiarid watersheds of the central Andes are governed by precipitation (36), we attribute the periods of slower erosion to periods of enhanced aridity.

Both slowdowns are synchronous with cold temperatures at high southern latitudes, as evidenced from glacial deposits, sea-surface temperatures, faunal assemblages, and benthic δ^{18}O records. We thus suggest that periods of aridity are associated with global glacial periods. The arid glacial periods proposed here are also synchronous with major faunal changes in South America: a shift from C3 to C4 vegetation in the latest Miocene (27) and a small-mammal extinction event in the middle Pliocene (49). Given that C4 plants can only outcompete C3 plants if aridity is also associated with lower atmospheric CO_2 levels, we suggest that the expansion of C4 vegetation may have been driven by low CO_2 rather than a shift toward warmer and wetter growing seasons. Regardless of the exact cause, it is clear that global climate is a first-order control on aridity and ecology in the south-central Andes and that large parts of the region experienced synchronous changes over time.

We speculate that aridity during glacial periods was caused by circulation changes in the SALLJ, which is responsible for delivering much of the modern moisture to the study area. Because the SALLJ depends on a baroclinic trough generated by interaction of westerly air masses with Andean topography, we hypothesize that a northward shift of the westerlies during glacial periods changed the location of this trough, thereby altering the geometry and/or intensity of the SALLJ.

Finally, our data show that paleo-erosion rates can be a powerful proxy for ancient continental climate, especially when ^{10}Be and ^{36}Cl are combined to reduce uncertainties associated with modern exposure. The inherent spatial and temporal averaging of sediment in a watershed yields a robust spatially averaged signal that can place tight temporal constraints on periods of continental aridity. When combined with appropriate global and regional climate proxies paleo-erosion rates may thus provide more precise information about the timing and amplitude of extreme climatic events that might otherwise be averaged out by marine-based proxies. In this case, our data pinpoint the timing of peak aridity to ~5.4 and 3.3 Ma, events that likely had a profound impact on the faunal evolution of the south-central Andes and neighboring regions.

ACKNOWLEDGMENTS. We thank Louise McCarren for field assistance and Ryan McElroy, C. C. Connard, and Andrew Hollyday for laboratory assistance. This work was supported by the NSF Geomorphology and Land Use Dynamics program through NSF Grant EAR-1148233.

1. Hewitt GM (2004) Genetic consequences of climatic oscillations in the Quaternary. *Philos Trans R Soc Lond B Biol Sci* 359:183–195, discussion 195.
2. deMenocal PB (2004) African climate change and faunal evolution during the Pliocene-Pleistocene. *Earth Planet Sci Lett* 220:3–24.
3. Zachos J, Pagani M, Sloan L, Thomas E, Billups K (2001) Trends, rhythms, and aberrations in global climate 65 Ma to present. *Science* 292:686–693.
4. Arakaki M, et al. (2011) Contemporaneous and recent radiations of the world's major succulent plant lineages. *Proc Natl Acad Sci USA* 108:8379–8384.
5. Dupont LM, Rommerskirchen F, Mollenhauer G, Schefuß E (2013) Miocene to Pliocene changes in South African hydrology and vegetation in relation to the expansion of C4 plants. *Earth Planet Sci Lett* 375:408–417.
6. Cerling TE, Wang Y, Quade J (1993) Expansion of C4 ecosystems as an indicator of global ecological change in the late Miocene. *Nature* 361:344–345.
7. Quade J, Cerling TE (1995) Expansion of C4 grasses in the Late Miocene of Northern Pakistan: Evidence from stable isotopes in paleosols. *Palaeogeogr Palaeoclimatol Palaeoecol* 115:91–116.
8. Ehleringer JR, Cerling TE, Helliker BR (1997) C4 photosynthesis, atmospheric CO_2, and climate. *Oecologia* 112:285–299.
9. Still CJ, Berry JA, Collatz GJ, DeFries RS (2003) Global distribution of C3 and C4 vegetation: Carbon cycle implications. *Global Biogeochem Cycles* 17: 6-1–6-14.
10. Pagani M, Freeman KH, Arthur MA (1999) Late miocene atmospheric CO(2) concentrations and the expansion of C(4) grasses. *Science* 285:876–879.
11. Freeman KH, Colarusso LA (2001) Molecular and isotopic records of C4 grassland expansion in the late miocene. *Geochim Cosmochim Acta* 65:1439–1454.
12. Bolton CT, Stoll HM (2013) Late Miocene threshold response of marine algae to carbon dioxide limitation. *Nature* 500:558–562.
13. Bolton CT, et al. (2016) Decrease in coccolithophore calcification and CO_2 since the middle Miocene. *Nat Commun* 7:10284.
14. Latorre C, Quade J, McIntosh WC (1997) The expansion of C4 grasses and global change in the late Miocene; stable isotope evidence from the Americas. *Earth Planet Sci Lett* 146:83–96.

15. Quade J, Cater JML, Ojha TP, Adam J, Harrison TM (1995) Late Miocene environmental change in Nepal and the northern Indian subcontinent: Stable isotopic evidence from paleosols. *Geol Soc Am Bull* 107:1381–1397.
16. Cosentino D, et al. (2013) Refining the Mediterranean "Messinian gap" with high-precision U-Pb zircon geochronology, central and northern Italy. *Geology* 41:323–326.
17. Pérez-Asensio JN, Aguirre J, Jiménez-Moreno G, Schmiedl G, Civis J (2013) Glacioeustatic control on the origin and cessation of the Messinian salinity crisis. *Global Planet Change* 111:1–8.
18. Garcia-Castellanos D, Villaseñor A (2011) Messinian salinity crisis regulated by competing tectonics and erosion at the Gibraltar arc. *Nature* 480:359–363.
19. Ohneiser C, et al. (2015) Antarctic glacio-eustatic contributions to late Miocene Mediterranean desiccation and reflooding. *Nat Commun* 6:8765.
20. Hilgen F, Kuiper K, Krijgsman W, Snel E, van der Laan E (2007) Astronomical tuning as the basis for high resolution chronostratigraphy: The intricate history of the Messinian Salinity Crisis. *Stratigraphy* 4:231–238.
21. Hodell DA, Curtis JH, Sierro FJ, Raymo ME (2001) Correlation of late Miocene to early Pliocene sequences between the Mediterranean and North Atlantic. *Paleoceanography* 16:164–178.
22. Hodell DA, Elmstrom KM, Kennett JP (1986) Latest miocene benthic $\delta^{18}O$ changes, global ice volume, sea level and the 'Messinian salinity crisis'. *Nature* 320:411–414.
23. Larsen HC, et al.; ODP Leg 152 Scientific Party (1994) Seven million years of glaciation in greenland. *Science* 264:952–955.
24. Mercer JH (1983) Cenozoic glaciation in the Southern Hemisphere. *Annu Rev Earth Planet Sci* 11:99–132.
25. Passey BH, Cerling TE (2006) In situ stable isotope analysis ($\delta^{13}C$, $\delta^{18}O$) of very small teeth using laser ablation GC/IRMS. *Chem Geol* 235:238–249.
26. Uno KT, Polissar PJ, Jackson KE, deMenocal PB (2016) Neogene biomarker record of vegetation change in eastern Africa. *Proc Natl Acad Sci USA* 113:6355–6363.
27. Hynek SA, et al. (2012) Small mammal carbon isotope ecology across the Miocene-Pliocene boundary, northwestern Argentina. *Earth Planet Sci Lett* 321-322:177–188.
28. Bywater-Reyes S, Carrapa B, Clementz M, Schoenbohm L (2010) Effect of late Cenozoic aridification on sedimentation in the Eastern Cordillera of northwest Argentina (Angastaco Basin). *Geology (Boulder)* 38:235–238.
29. Fosdick JC, Carrapa B, Ortíz G (2015) Faulting and erosion in the Argentine Precordillera during changes in subduction regime: Reconciling bedrock cooling and detrital records. *Earth Planet Sci Lett* 432:73–83.
30. Jordan TE, et al. (2001) Unsteady and spatially variable evolution of the Neogene Andean Bermejo foreland basin, Argentina. *J S Am Earth Sci* 14:775–798.
31. Jordan TE, Allmendinger RW, Damanti JF, Drake RE (1993) Chronology of motion in a complete thrust belt: The Precordillera, 30-31 degrees S, Andes Mountains. *J Geol* 101: 135–156.
32. Coughlin TJ, O'Sullivan PB, Kohn BP, Holcombe RJ (1988) Apatite fission-track thermochronology of the Sierras Pampeanas, central western Argentina: Implications for the mechanism of plateau uplift in the Andes. *Geology* 26:999–1002.
33. Strecker MR, et al. (2007) Tectonics and climate of the southern central Andes. *Annu Rev Earth Planet Sci* 35:747–787.
34. Pingel H, et al. (2014) Pliocene orographic barrier uplift in the southern Central Andes. *Geology* 42:691–694.
35. Rohrmann A, et al. (2016) Miocene orographic uplift forces rapid hydrological change in the southern central Andes. *Sci Rep* 6:35678.
36. Bookhagen B, Strecker MR (2012) Spatiotemporal trends in erosion rates across a pronounced rainfall gradient: Examples from the southern Central Andes. *Earth Planet Sci Lett* 327-328:97–110.
37. Charreau J, et al. (2011) Paleo-erosion rates in Central Asia since 9Ma: A transient increase at the onset of Quaternary glaciations? *Earth Planet Sci Lett* 304:85–92.
38. Val P, Hoke GD, Fosdick JC, Wittmann H (2016) Reconciling tectonic shortening, sedimentation and spatial patterns of erosion from ^{10}Be paleo-erosion rates in the Argentine Precordillera. *Earth Planet Sci Lett* 450:173–185.
39. Puchol N, et al. (2016) Limited impact of Quaternary glaciations on denudation rates in Central Asia. *Geol Soc Am Bull* 129:479–499.
40. Amidon WH, et al. (2016) U-Pb ages of detrital and volcanic zircons of the Toro Negro Formation, northwestern Argentina: Age, provenance and sedimentation rates. *J S Am Earth Sci* 70:237–250.
41. Ruskin BG, Jordan TE (2007) Climate change across continental sequence boundaries: Paleopedology and lithofacies of Iglesia Basin, northwestern Argentina. *J Sediment Res* 77:661–679.
42. Peck DM, Missimer TM, Slater DH, Wise SW, Jr, O'Donnell TH (1979) Late Miocene glacial-eustatic lowering of sea level: Evidence from the Tamiami Formation of South Florida. *Geology (Boulder)* 7:285–288.
43. Loutit TS, Keigwin LD, Jr (1982) Stable isotopic evidence for latest Miocene sea-level fall in the Mediterranean region. *Nature* 300:163–166.
44. Loutit TS, Kennett JP (1979) Application of carbon isotope stratigraphy to late miocene shallow marine sediments, new zealand. *Science* 204:1196–1199.
45. Shackleton NJ, Kennett JP (1975) Late Cenozoic oxygen and carbon isotopic changes at DSDP Site 284: Implications for glacial history of the Northern Hemisphere and Antarctica. *Initial Rep Deep Sea Drill Proj* 29:801–807.
46. Hayes DE, Frakes LA (1975) General synthesis, Deep Sea Drilling Project Leg 28. *Initial Rep Deep Sea Drill Proj* 28:919–942.
47. Lisiecki LE, Raymo ME (2005) A Pliocene-Pleistocene stack of 57 globally disturbed benthic $\delta^{18}O$ records. *Paleoceanography* 20:PA1003.
48. Mercer JH (1976) Glacial history of southernmost South America. *Quat Res* 6:125–166.
49. Vizcaino SF, Farina RA, Zarate MA, Bargo MS, Schultz P (2004) Palaeoecological implications of the mid-Pliocene faunal turnover in the Pampean region (Argentina). *Palaeogeogr Palaeoclimatol Palaeoecol* 213:101–113.
50. Schultz PH, Zarate M, Hames W, Camilion C, King J (1998) A 3.3-Ma impact in argentina and possible consequences. *Science* 282:2061–2063.
51. Ortiz PE, et al. (2012) Exceptional late Pliocene microvertebrate diversity in northwestern Argentina reveals a marked small mammal turnover. *Palaeogeogr Palaeoclimatol Palaeoecol* 361-362:21–37.
52. Hodell DA, Venz K (1992) Toward a high-resolution stable isotopic record of the Southern Ocean during the Pliocene-Pleistocene (4.8 to 0.8 Ma). *The Antarctic Paleoenvironment: A Perspective on Global Change: Part One*, eds Kennett JP, Warkne DA (American Geophysical Union, Washington, DC), Vol 56, pp 265–310.
53. Kennett JP, Hodell DA (1993) Evidence for relative climatic stability of Antarctica during the early Pliocene: A marine perspective. *Geogr Ann, Ser A* 75:205–220.
54. Bohaty SM, Harwood DM (1998) Southern Ocean Pliocene paleotemperature variation from high-resolution silicoflagellate biostratigraphy. *Mar Micropaleontol* 33: 241–272.
55. Keany J (1978) Paleoclimatic trends in early and middle Pliocene deep-sea sediments of the Antarctic. *Mar Micropaleontol* 3:35–49.
56. Ciesielski PF, Grinstead GP (1986) Pliocene variations in the position of the Antarctic convergence in the Southwest Atlantic. *Paleoceanography* 1:197–232.
57. Barron JA (1996) Diatom constraints on the position of the Antarctic Polar Front in the middle part of the Pliocene. *Mar Micropaleontol* 27:195–213.
58. Garreaud RD, Vuille M, Compagnucci R, Marengo J (2009) Present-day South American climate. *Palaeogeogr Palaeoclimatol Palaeoecol* 281:180–195.
59. Romatschke U, Houze RA, Jr (2010) Extreme summer convection in South America. *J Clim* 23:3761–3791.
60. Castañeda ME, Ulke AG (2015) Analysis of atmospheric conditions associated to CHACO events of the Low Level Jet East of the Andes and their implications for regional transport. *Int J Climatol* 35:4126–4138.
61. Rohrmann A, et al. (2014) Can stable isotopes ride out the storms? The role of convection for water isotopes in models, records, and paleoaltimetry studies in the central Andes. *Earth Planet Sci Lett* 407:187–195.
62. Nicolini M, Saulo AC (2006) Modeled Chaco low-level jets and related precipitation patterns during the 1997-1998 warm season. *Meteorol Atmos Phys* 94:129–143.
63. Salio P, Nicolini M, Saulo AC (2002) Chaco low-level jet events characterization during the austral summer season. *J Geophys Res, D, Atmospheres* 107:ACL 32-1–ACL 32-17.
64. Campetella CM, Vera CS (2002) The influence of the Andes mountains on the South American low-level flow. *Geophys Res Lett* 29:7-1–7-4.
65. Marengo JA (2004) Interdecadal variability and trends of rainfall across the Amazon basin. *Theor Appl Climatol* 78:79–96.
66. Wang H, Fu R (2004) Influence of cross-Andes flow on the South American low-level jet. *J Clim* 17:1247–1262.
67. Marengo JA, Soares WR, Saulo C, Nicolini M (2004) Climatology of the low-level jet east of the Andes as derived from the NCEP-NCAR reanalyses: Characteristics and temporal variability. *J Clim* 17:2261–2280.
68. Moreno PI, Lowell TV, Jacobson GL, Jr, Denton GH (1999) Abrupt vegetation and climate changes during the Last Glacial Maximum and last termination in the Chilean Lake District: A case study from Canal de la Puntilla (41°S). *Geogr Ann, Ser A* 81: 285–311.
69. Stuut JBW, Lamy F (2004) Climate variability at the southern boundaries of the Namib (southwestern Africa) and Atacama (northern Chile) coastal deserts during the last 120,000 yr. *Quat Res* 62:301–309.
70. Toggweiler JR, Russell JL, Carson SR (2006) Midlatitude westerlies, atmospheric CO_2, and climate change during the ice ages. *Paleoceanography* 21, 10.1029/2005PA001154.
71. Thompson DWJ, Solomon S (2002) Interpretation of recent Southern Hemisphere climate change. *Science* 296:895–899.
72. Saulo C, Ruiz J, García Skabar Y (2007) Synergism between the low-level jet and organized convection at its exit region. *Mon Weather Rev* 135:1310–1326.
73. Goss AR, Kay SM, Mpodozis C (2013) Andean adakite-like high-Mg andesites on the northern margin of the Chilean-Pampean flat-slab (27–28.5° S) associated with frontal arc migration and fore-arc subduction erosion. *J Petrol* 54:2193–2234.
74. Kay SM, Mpodozis C, Gardeweg M (2013) Magma sources and tectonic setting of Central Andean andesites (25.5°–28° S) related to crustal thickening, forearc subduction erosion and delamination. Special Publication (Geological Society of London, London), Vol 385, pp 303–334.
75. Allmendinger RW, Judge PA (2014) The Argentine Precordillera: A foreland thrust belt proximal to the subducted plate. *Geosphere* 10:1203–1218.
76. Mercer JH, Sutter JF (1982) Late Miocene-earliest Pliocene glaciation in southern Argentina: Implications for global ice-sheet history. *Palaeogeogr Palaeoclimatol Palaeoecol* 38:185–206.